

Kinetic Model of the Photocatalytic Effect of a Photosystem I Monolayer on a Planar Electrode Surface

Peter N. Ciesielski,^{*,†} David E. Cliffel,^{†,‡} and G. Kane Jennings^{†,§}

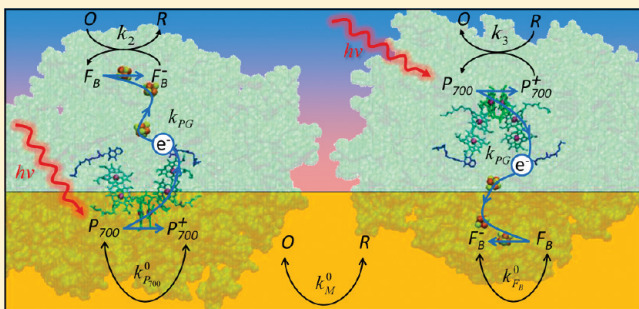
[†]Interdisciplinary Materials Science Program, Vanderbilt University, VU Station B 350106, 2301 Vanderbilt Place, Nashville, Tennessee 37234-0106, United States

[§]Department of Chemical and Biomolecular Engineering, Vanderbilt University, 2400 Highland Avenue, 107 Olin Hall, Nashville, Tennessee 37212, United States

[‡]Department of Chemistry, Vanderbilt University, 7330 Stevenson Center, VU Station B 351822, Nashville, Tennessee 37235, United States

 Supporting Information

ABSTRACT: Photosystem I (PSI), a photoactive protein complex that participates in the light reactions of natural photosynthesis, can exhibit photocatalytic capabilities when incorporated to electrochemical systems. Here we present a simulation for the photoelectrochemical behavior of an electrode modified with a monolayer of Photosystem I complexes during photochronoamperometric experiments in which the electrode is exposed to periods of darkness and irradiation. A kinetic model is derived from conservation statements for the various oxidation states of the reaction centers of PSI complexes and electrochemical mediators within the system. The kinetic parameters that dictate the performance of the simulation are extracted from experimental data and the resulting simulation is capable of predicting the photochronoamperometric behavior of the system over a range of overpotentials. The model is used to investigate the various contributions to the photocurrent production of the system as well as the effects of the orientation of PSI complexes adsorbed to the electrode surface.



In this work, we develop a mechanistic model for the photocatalytic effect produced by a monolayer of PSI complexes adsorbed onto a planar electrode surface and compare the simulated current density produced by the model to experimental photochronoamperometric data. Previous studies have shown that PSI complexes assembled at electrode interfaces may interact electrochemically with the electrode surface directly as well as with electrochemical mediators in the electrolyte.^{6–8,17} The heterogeneous electron transfer events that occur in these systems may be precisely monitored by analytical electrochemical methods, which makes the PSI-modified electrode system an ideal platform for analysis of the protein's photocatalytic behavior by the application of a mechanistic model. A model for the steady state electron transfer between PSI complexes suspended in solution and cytochrome c6 assembled at the electrode surface was previously developed by Proux-Delrouyre and colleagues.¹⁸ While that study demonstrated an insightful method by which electrochemical measurements, mainly cyclic voltammograms, may be used to extract information about the steady-state kinetics and bioenergetics of biological redox couples, it did not describe direct

INTRODUCTION

Photosynthesis is the natural solar energy conversion process employed by plants and certain types of bacteria and accounts for the annual conversion of 10^{11} metric tons of CO₂ to organic matter, which equates to a storage of 4×10^{21} J of free energy in the form of reduced carbon.¹ This process is performed by several protein complexes that operate in tandem to photocatalyze the electrochemical reactions that drive photosynthesis. One of these proteins, Photosystem I (PSI), exhibits particularly useful functionality in capturing and converting solar energy. With a quantum efficiency near unity,² the protein complex operates as a photodiode for the transport of electrons across the thylakoid membrane on a time scale of $\sim 1\ \mu\text{s}$,³ and the reduction potentials achieved by PSI's iron–sulfur complexes are among the most negative found in nature.⁴ Improvements in nanofabrication as well as biochemical techniques in the last several decades have produced studies that have demonstrated PSI's utility in biohybrid electrochemical^{5–10} and solid-state^{11–16} systems. As PSI emerges as a vastly abundant biological resource with promising efficacy, its photoelectrochemical performance must be thoroughly described both qualitatively and quantitatively so that its interactions with otherwise non-biological system components may be well understood and accurately predicted.

Received: January 5, 2011

Revised: March 13, 2011

Published: March 30, 2011

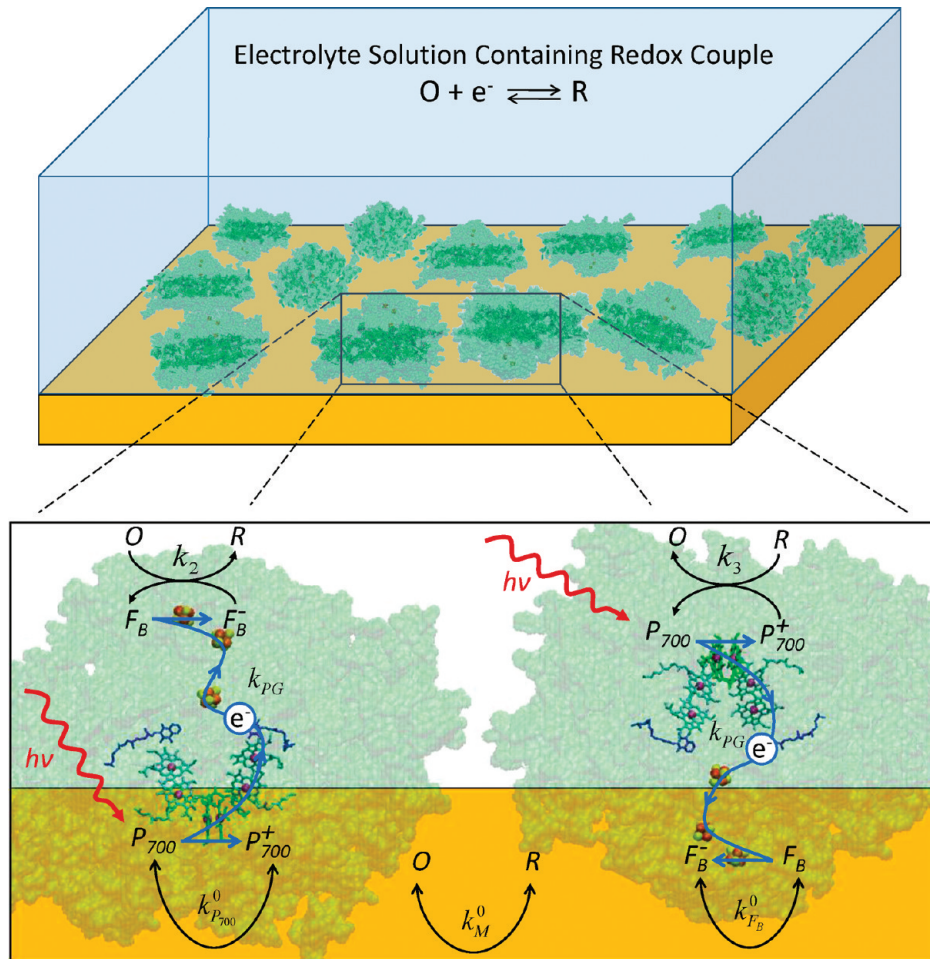


Figure 1. A monolayer of PSI complexes on an electrode surface will photocatalyze redox reactions in the presence of an electrolyte that contains a redox couple that is suitable to act as an electrochemical mediator. Zoom window: In dark conditions, a baseline current flows due to heterogeneous reactions of the redox couple. When the electrode is irradiated, energy from photons is collected by chlorophylls coordinated within PSI and transferred to the special pair of chlorophylls that compose the P_{700} reaction center. The reaction center is quickly oxidized to P_{700}^+ as it releases an electron into an energy cascade of intraprotein cofactors. The electron may travel through either of the cofactor branches to eventually arrive at PSI's terminal electron acceptor, an iron–sulfur complex denoted as F_B , which is reduced to F_B^- . An oxidized P_{700}^+ may be reduced back to P_{700} by a reduced mediator; similarly, a reduced F_B^- may be oxidized back to F_B by an oxidized mediator. The PSI complex on the left is oriented such that its P_{700} reaction center is electronically accessible to the underlying electrode, while that on the right is oriented such its F_B iron sulfur complex is electronically accessible to the electrode. Atomic coordinates for the representations of PSI complexes used in this figure were contributed by Amunts et al.,²² PDB entry 2O01.

electrochemical interactions between PSI and the electrode surface, nor did it investigate the transient behavior of the system when the irradiation conditions change abruptly. Much of the attraction of PSI is that its rapid, photoinduced electron transfer capabilities may be interfaced with nonbiological materials. Thus, additional quantitative characterization of the photoelectrochemical behavior of systems that make use of PSI complexes adsorbed at an electrode/electrolyte interface is pertinent to the design of future biohybrid technologies and devices that utilize PSI, and such is the focus of the present study.

A schematic of a PSI monolayer on an electrode surface is shown in Figure 1. Chlorophylls oriented within PSI absorb energy from photons and transfer it to a special pair of chlorophylls that make up the P_{700} reaction center. Receipt of this energy causes the reaction center to achieve an excited state denoted P_{700}^* , which is quickly oxidized to P_{700}^+ as it releases an electron into an energy cascade of intraprotein cofactors made up of chlorophylls and phylloquinones that transfer the electron to iron sulfur complexes located on the stromal side of the protein. The terminal electron acceptor of this electron transfer chain is an iron sulfur complex

denoted F_B , which is reduced to F_B^- when the electron arrives. In natural photosynthesis, F_B^- is oxidized by chloroplast ferredoxin, and electrons are resupplied to P_{700}^+ by plastocyanin. However, in the absence of PSI's naturally occurring redox partners, the reduction potentials of F_B^- and P_{700}^+ (-0.58 and $+0.49$ V vs NHE, respectively) allow them to react with many xenobiotic compounds including viologens,¹⁹ metal salts, and coordination compounds.^{10,20} The $K_3Fe(CN)_6/K_4Fe(CN)_6$ redox couple was chosen as the electrochemical mediator for this study because its redox potential (~ 0.36 – 0.45 V vs NHE)²¹ allows its oxidized and reduced forms to react with F_B^- and P_{700}^+ , respectively. For simplicity during the discussion of the remainder of this manuscript, the oxidized form of this redox couple, $Fe(CN)_6^{3-}$, will be referred to as O , and the reduced form, $Fe(CN)_6^{4-}$, will be referred to as R .

METHODS

Model Description. The net current density measured from a PSI-modified electrode during a chronoamperometric experiment is

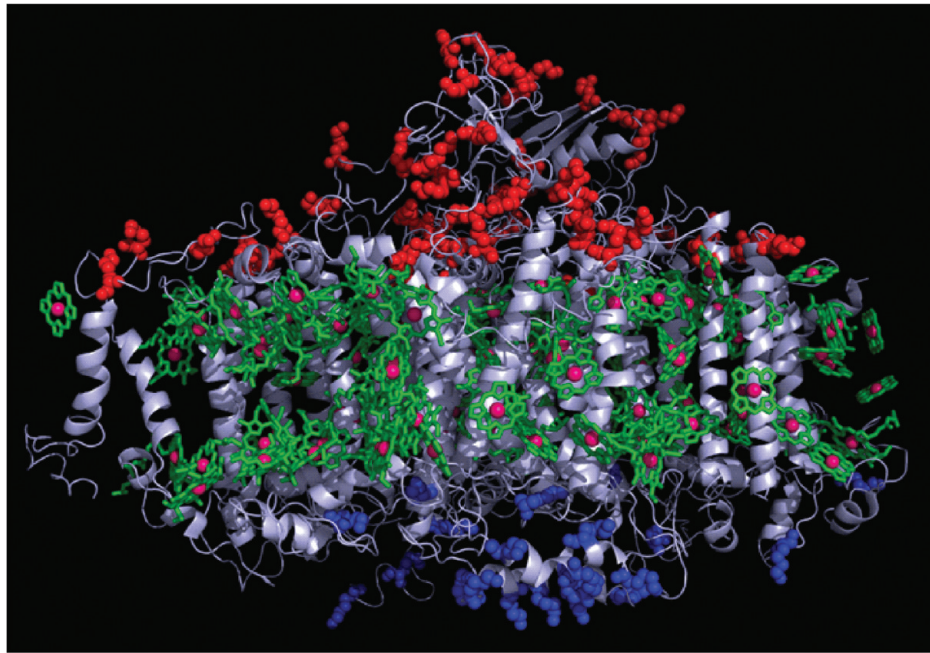


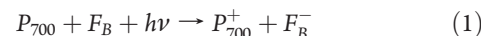
Figure 2. Structural model of PSI reveals that lysine residues are present on both the luminal and stromal side of the protein complex (lysine residues located on the stromal side of PSI are highlighted in red, while those on the luminal side are shown in blue; color available online). The attachment scheme employed to immobilize PSI on the electrode surface covalently binds lysine residues on the protein to functional groups of the SAM. The orientation of PSI complexes on the electrode surface was assumed to be proportional to the distribution of these residues on the protein. Atomic coordinates for the structure of PSI used in this figure were contributed by Amunts et al.,²² PDB entry 2O01.

determined by the rates of the heterogeneous redox reactions occurring at the electrode and thus, contains contributions from electron transfer between the electrode and the electrochemical mediator in the electrolyte as well as electron transfer between the electrode and the reaction centers of adsorbed PSI complexes as shown in Figure 1. These reactions were modeled using an interface balance similar to the method described by Deen,²³ wherein conservation statements for the heterogeneous reactants are evaluated at the electrode/electrolyte interface. This approach was extended to an electrode modified by a PSI monolayer by considering the system to contain three redox couples: the mobile electrochemical mediator consisting of the O/R redox couple, and two adsorbed (immobile) redox couples, P_{700}^+/P_{700} and F_B/F_B^- , that correspond to the reaction centers of PSI complexes. These three redox couples were assumed to participate in heterogeneous electron transfer reactions with the electrode and with each other as shown schematically in Figure 1, and kinetic descriptions of these reactions were developed. These kinetic descriptions of charge transfer events that involve the reaction centers of PSI are developed in the main text of this work, while those primarily involving the electrochemical mediators are presented in Supporting Information.

In this study, dense monolayers of PSI were prepared by exposing a suspension of the protein to gold surfaces that were modified by self-assembled monolayers of aminoethanethiol that were further functionalized with terephthalaldehyde.⁶ The aldehyde terminal groups of this SAM form covalent bonds with the lysine residues on the exterior of PSI, which anchors the protein to the electrode surface.^{6,7} Lysine residues are found on the hydrophilic regions of PSI, on both the stromal and luminal regions as shown in Figure 2. Excluding the light-harvesting subunits, the structure of plant PSI contains ~ 88 lysine residues, 24 of which are located on the luminal side, and the remaining 64 are found on the stromal side.²² Based on this attachment scheme, we assumed that

the P_{700} site of PSI complexes bound to the surface via lysine residues on the luminal side (highlighted in blue in Figure 2) was electronically accessible to the electrode (see PSI complex on left of Figure 1 zoom window), and that the F_B site of PSI complexes bound to the surface via lysine residues on the stromal side (highlighted in red in Figure 2) was electronically accessible to the electrode (see PSI complex on right of Figure 1 zoom window). In addition, the orientation of PSI complexes in the monolayer was assumed to be proportional to the number of lysine residues on each side, thus, 27% were assumed oriented with their P_{700} sites accessible to the electrode and 73% were oriented with their F_B sites accessible. Some discrepancy exists between the dimensions of PSI as measured by TEM,²⁴ AFM,²⁵ and STM,²⁶ yet all of these studies place the major axis of the protein between 6 and 14 nm, and the minor axis between 5 and 12 nm. For this model, we assumed the footprint of a single PSI complex in a dense monolayer to be $\sim 80\text{ nm}^2$, which corresponds to an ellipse of major and minor axes 12 and 8.5 nm, respectively, and an approximate surface concentration, denoted Γ_{PSI} , of $2 \times 10^{-12}\text{ mol/cm}^2$.

Photogeneration of the F_B^- and P_{700}^+ sites requires the absorption of photons by chlorophylls within PSI, as well as P_{700} reaction centers in the reduced state to donate electrons into their corresponding electron transfer chains, and F_B sites in the oxidized state to receive these electrons. While, in reality, this event is not an elementary step and proceeds via an electron transfer chain made up of several cofactors and FeS intermediates, for the purpose of this analysis, the overall reaction was simplified to



Electron transfer within PSI is generally accepted to proceed as $F_X \rightarrow F_A \rightarrow F_B$,^{27,28} thus, we assumed that only the F_B FeS complex could act as the terminal electron acceptor in the model. We⁷ and others⁸ have observed the photocurrent responses

of PSI modified electrodes to be proportional to the intensity of the irradiation incident at the electrode surface. Thus, considering the photogeneration reaction as described by eq 1 is advantageous because it allows photons in this system to be treated as reactants on a molar basis. For irradiation by light of a single wavelength λ , we propose a general rate expression to describe the photogeneration of F_B^- and P_{700}^+ sites in units of [$\text{mols} \cdot \text{cm}^{-2} \cdot \text{s}^{-1}$] given by:

$$r_1(\lambda) = N_\lambda \theta_\lambda \eta_{IQ} k_{PG} \Gamma_{P_{700}} \Gamma_{F_B} \quad (2)$$

where N_λ is the flux of photons of wavelength λ at the electrode surface in units of [$\text{mols} \cdot \text{cm}^{-2} \cdot \text{s}^{-1}$], θ_λ is the fraction of those incident photons that are absorbed by the PSI complexes on the electrode surface, and η_{IQ} is the internal quantum efficiency of PSI (i.e., the probability that the absorbed photon will initiate charge separation, which is conservatively estimated as 95%),^{2,29} and k_{PG} is a proportionality constant with units of [$\text{cm}^4 \cdot \text{mol}^{-2}$] that relates the photonic flux to the photogeneration of F_B^- and P_{700}^+ sites. Assuming that $\Gamma_{P_{700}^+} + \Gamma_{P_{700}} = \Gamma_{F_B^-} + \Gamma_{F_B} = \Gamma_{PSI}$, eq 2 can be rewritten as

$$r_1(\lambda) = N_\lambda \theta_\lambda \eta_{IQ} k_{PG} (\Gamma_{PSI} - \Gamma_{P_{700}^+}) (\Gamma_{PSI} - \Gamma_{F_B^-}) \quad (3)$$

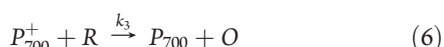
to ensure the number of photogenerated F_B^- and P_{700}^+ sites does not exceed the number of reaction centers provided by PSI complexes present in the system.

Consumption of F_B^- and P_{700}^+ sites may occur by their oxidation and reduction, respectively, by the electrochemical mediator and by the electrode directly. In addition, charge recombination between F_B^- and P_{700}^+ may consume these photogenerated states; however, this process is orders of magnitude slower than photo-induced charge separation³⁰ and was thus considered to be negligible in the present model. While it has been shown that charge recombination between F_X^- and P_{700}^+ can occur significantly faster than charge recombination between F_B^- and P_{700}^+ when the terminal acceptor of the electron transfer chain is in the reduced state, this process occurs in 0.45–1.5 ms,³¹ which is still ~ 3 orders of magnitude slower than the charge separation process and was similarly neglected. The reduction of a mediator in the oxidized state by F_B^- is described by the following chemical equation and corresponding rate expression



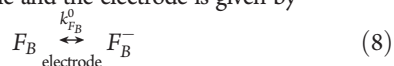
$$r_2 = k_2 \Gamma_{F_B^-} C_{O,(x=0)} \quad (5)$$

where $C_{O,(x=0)}$ is the concentration of the oxidized form of the electrochemical mediator at the electrode surface, which requires that the rate constant k_2 carry units of [$\text{cm}^3 \cdot \text{mol}^{-1} \cdot \text{s}^{-1}$]. Similarly, the oxidation of a mediator in the reduced state by P_{700}^+ is described by the following chemical equation and rate expression:



$$r_3 = k_3 \Gamma_{P_{700}^+} C_{R,(x=0)} \quad (7)$$

where k_3 also carries units of [$\text{cm}^3 \cdot \text{mol}^{-1} \cdot \text{s}^{-1}$]. In addition to the above redox reactions, PSI's reaction centers can interact with the electrode surface directly, provided that the protein complexes are oriented such that their reaction centers are electronically accessible. The chemical equation that describes the electron transfer events between the F_B/F_B^- couple and the electrode is given by



where $k_{F_B}^0$ is the standard rate constant of the couple. The rate expressions for the oxidation of F_B^- and reduction of F_B by the electrode

were obtained using a Butler–Volmer expression to account for the dependence of the rate upon the electrode potential to yield

$$r_4 = k_{F_B}^0 \exp[-\alpha_{F_B} f(E - E_{F_B}^{0'})] \chi_{down} \Gamma_{F_B} \quad (9)$$

for the reduction of F_B by the electrode and

$$r_5 = k_{F_B}^0 \exp[(1 - \alpha_{F_B})f(E - E_{F_B}^{0'})] \chi_{down} \Gamma_{F_B^-} \quad (10)$$

for the oxidation F_B^- of by the electrode, where χ_{down} is the fraction of PSI complexes oriented with their electron transport vectors pointing into the electrode, α_{F_B} is the transfer coefficient of the F_B/F_B^- redox couple, f is defined as F/RT and carries units of [V^{-1}], and the term $(E - E_{F_B}^{0'})$ is the difference between the formal potential for the redox couple and the applied electrode potential.³² Similarly, the chemical equation describing the interactions of the P_{700}^+/P_{700} couple and the electrode can be written as



which yields the Butler–Volmer rate expressions

$$r_6 = k_{P_{700}}^0 \exp[-\alpha_{P_{700}} f(E - E_{P_{700}}^{0'})] \chi_{up} \Gamma_{P_{700}^+} \quad (12)$$

and

$$r_7 = k_{P_{700}}^0 \exp[(1 - \alpha_{P_{700}})f(E - E_{P_{700}}^{0'})] \chi_{up} \Gamma_{P_{700}} \quad (13)$$

for the reduction of P_{700}^+ and oxidation of P_{700} by the electrode, respectively, where $k_{P_{700}}^0$ and $\alpha_{P_{700}}$ are the standard rate constant and transfer coefficient of the couple, respectively, and χ_{up} is the fraction of PSI complexes oriented with the electron transport chains pointing away from the electrode surface. These expressions describing the generation and consumption of PSI's reaction centers may be combined to yield the following time-dependent conservation statements for F_B^- and P_{700}^+ , respectively:

$$\begin{aligned} \frac{d\Gamma_{F_B^-}}{dt} &= N_\lambda \theta_\lambda \eta_{IQ} k_{PG} (\Gamma_{PSI} - \Gamma_{P_{700}^+}) (\Gamma_{PSI} - \Gamma_{F_B^-}) \\ &+ k_{F_B}^0 \exp[-\alpha_{F_B} f(E - E_{F_B}^{0'})] \chi_{down} \Gamma_{F_B} - k_2 \Gamma_{F_B^-} C_{O,(x=0)} \\ &- k_{F_B}^0 \exp[(1 - \alpha_{F_B})f(E - E_{F_B}^{0'})] \chi_{down} \Gamma_{F_B^-} \end{aligned} \quad (14)$$

$$\begin{aligned} \frac{d\Gamma_{P_{700}^+}}{dt} &= N_\lambda \theta_\lambda \eta_{IQ} k_{PG} (\Gamma_{PSI} - \Gamma_{P_{700}^+}) (\Gamma_{PSI} - \Gamma_{F_B^-}) \\ &+ k_{P_{700}}^0 \exp[(1 - \alpha_{P_{700}})f(E - E_{P_{700}}^{0'})] \chi_{up} \Gamma_{P_{700}} - k_3 \Gamma_{P_{700}^+} C_{R,(x=0)} \\ &- k_{P_{700}}^0 \exp[-\alpha_{P_{700}} f(E - E_{P_{700}}^{0'})] \chi_{up} \Gamma_{P_{700}^+} \end{aligned} \quad (15)$$

The surface concentrations $\Gamma_{F_B^-}$ and $\Gamma_{P_{700}^+}$ were assumed to be zero at the start of the experiment until the system was irradiated, which yields the initial conditions $\Gamma_{F_B^-}|_{t=0} = 0$ and $\Gamma_{P_{700}^+}|_{t=0} = 0$ for the differential eqs 14 and 15, respectively. To completely specify the system, conservation statements were also developed for the concentrations of the reduced and oxidized form of the redox couple. Diffusion of this mobile redox couple was described using statements of Fick's Second Law.²³ These partial differential equations, along with their boundary and initial conditions, are developed and presented in Supporting Information.

The time-dependent concentrations of the various redox couples at the electrode surface were obtained from the solution to these equations and used to back-calculate the net electron flux across the electrode/electrolyte interface. This electron flux corresponds to the current density that would be measured during a photochronoamperometric experiment and is calculated as

$$j_{\text{net}} = F[\sum \text{rate of heterogenous reduction events} - \sum \text{rate of heterogenous oxidation events}] \quad (16)$$

$$= F \left(\begin{array}{l} k_{P_{700}}^0 \exp[-\alpha_{P_{700}} f(E - E_{P_{700}}^0)] \chi_{\text{up}} \Gamma_{P_{700}^+} + k_{RC}^0 \exp[-\alpha_{RC} f(E - E_{RC}^0)] C_{O,(x=0)} \\ + k_{F_B}^0 \exp[-\alpha_{F_B} f(E - E_{F_B}^0)] \chi_{\text{down}} \Gamma_{F_B^-} - k_{F_B}^0 \exp[(1 - \alpha_{F_B}) f(E - E_{F_B}^0)] \chi_{\text{down}} \Gamma_{F_B^-} \\ - k_{RC}^0 \exp[(1 - \alpha_{RC}) f(E - E_{RC}^0)] C_{R,(x=0)} - k_{P_{700}}^0 \exp[(1 - \alpha_{P_{700}}) f(E - E_{P_{700}}^0)] \chi_{\text{up}} \Gamma_{P_{700}} \end{array} \right) \quad (17)$$

Note that this equation only contains contributions from electrochemical reactions that involve the electrode surface directly (terms in eq 17 containing Butler–Volmer expressions for electron transfer between the electrode and the electrochemical mediator are described in Supporting Information).

■ EXPERIMENTAL SECTION

Photosystem I Extraction. PSI-40 complexes were extracted from commercial baby spinach as described previously,³³ and then purified by an additional dialysis step. To briefly summarize the procedure, thylakoid membranes were isolated via maceration followed by centrifugation using the method of Reeves et al.³⁴ with several adaptations.³⁵ PSI complexes were then separated from the thylakoid membranes by additional centrifugation followed by purification using a chromatographic column packed with hydroxylapatite.^{36,37} The column effluent was then dialyzed in deionized water for 24 h using 10000 MWCO dialysis tubing (Spectrapore). The total chlorophyll concentration of the product was determined by the method of Porra et al.³⁸ to be 7.1×10^{-5} M with a Chl *a*/Chl *b* ratio of 3.3, and the P₇₀₀ concentration was determined using the method of Baba et al.³⁶ to be 1.6×10^{-6} M, yielding a Chl/P₇₀₀ ratio of 43.

PSI-Modified Electrode Preparation. Au/Si substrates were prepared by thermally evaporating 125 nm of Au (J&J Materials) onto silicon wafers (Montico Silicon, {100} orientation, 100 mm diameter, 500–550 mm thick) with a 10 nm adhesion layer of Cr (R.D. Mathis). Samples were cut to approximately 1.3 × 2 cm. Covalently attached PSI monolayers were formed by solution adsorption on to a functionalized SAM as described previously.⁶ In summary, the procedure consisted of the preparation of amine-terminated SAMs prepared by exposing the gold surface to a 1 mM ethanolic solution of the adsorbate for 12 h, and then further modification of the SAM by exposing the surface to 1 mM solution of terephthalaldehyde (Aldrich) for 1 h. The functionalized gold surface was then exposed to the dialyzed PSI suspension for 48 h at 4 °C, after which it was rinsed with deionized water and dried with nitrogen to yield a dense, covalently attached PSI monolayer on the surface of the substrate.

Photoelectrochemical Characterization. All electrochemical measurements were taken with a CH Instruments CHI660a electrochemical workstation equipped with a Faraday cage. Experiments were performed using a custom-made electrochemical cell in a three-electrode configuration, with the PSI-modified substrate serving as the working electrode, an Ag/AgCl reference electrode, and a Pt mesh counterelectrode. The electrolyte solution consisted of 100 μM K₃Fe(CN)₆, 100 μM K₄Fe(CN)₆, and 0.1 M KCl in pH 7 phosphate buffered solution. The light source employed was a Gebrauch KL 2500 LCD lamp, and a red filter was employed to minimize background photocurrent contributions from the mediator solution. The power output of this light source was measured using an Ophir Orion-TH power

meter equipped with a thermal detector head, and the emission spectrum was collected using an Ocean Optics USB 2000 fiber optic spectrometer. This emission spectrum is presented in Figure S1 in Supporting Information.

■ RESULTS AND DISCUSSION

Experimental Results. To extract the kinetic parameters that govern the previously described model, we performed photochronoamperometric experiments over a range of working electrode potentials (Figure 3). Equimolar concentrations of each species of the redox couple were used, and the resulting equilibrium potential of the electrolyte solution was observed to be 0.212 V versus Ag/AgCl, which is very close to the formal potential of the redox couple (~0.227 V vs Ag/AgCl),²¹ as predicted by the Nernst equation. Defining the overpotential as $\eta = E_w - E_{eq}$, where E_w is the working electrode potential and E_{eq} is the equilibrium potential, all experiments performed at positive overpotentials display an anodic (negative) baseline current, while those performed at negative overpotentials display a cathodic (positive) baseline current. The curvature observed in the current density measured during these experiments results from the formation of gradients in the concentration of the heterogeneous reactant (i.e., the electrochemical mediator) that propagates away from the electrode as the reactant is consumed

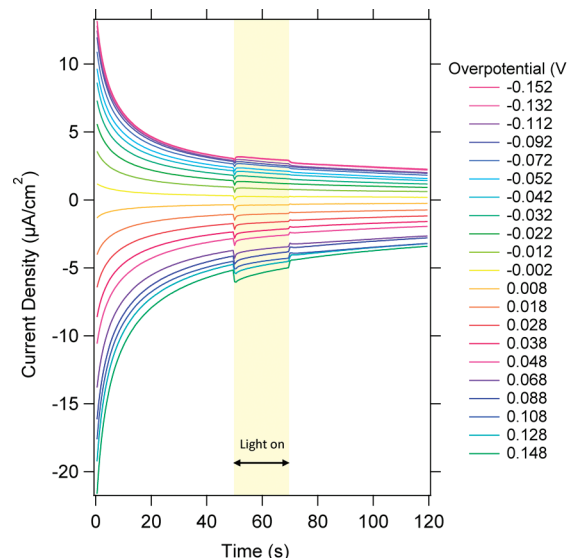


Figure 3. Photochronoamperometric experiments were performed over a range of overpotentials using a working electrode modified with a PSI monolayer. Irradiation of the electrode produced photocurrents whose magnitude and direction were dependent on the overpotential. Negative overpotentials cause positive, or cathodic, baseline currents to flow, while positive overpotentials induce negative, or anodic, baseline currents. Kinetic parameters were empirically obtained from this data set by iteratively varying the parameters to minimize the residual between the simulated and experimental current densities.

Table 1. Parameters Extracted from Experimental Data

parameter	chemical equation	parameter value [units]
k_{PG}	$P_{700} + F_B + h\nu \xrightarrow{k_{PG}} P_{700}^+ + F_B^-$	$1.8 \pm 0.5 \times 10^{23}$ [cm ⁴ ·mol ⁻²]
k_M^0	$O \leftrightarrow \text{electrode}^k M$	$9.6 \pm 0.5 \times 10^{-4}$ [cm·s ⁻¹]
$k_{F_B}^0$	$F_B^- \leftrightarrow \text{electrode}^k F_B$	53 ± 4 [s ⁻¹]
$k_{P_{700}}^0$	$P_{700}^+ \leftrightarrow \text{electrode}^k P_{700}$	$1.2 \pm 0.1 \times 10^2$ [s ⁻¹]
k_2	$F_B^- + O \xrightarrow{k_2} F_B + R$	$7.8 \pm 2.0 \times 10^{11}$ [cm ³ ·mol ⁻¹ ·s ⁻¹]
k_3	$P_{700}^+ + R \xrightarrow{k_3} P_{700} + O$	$7.4 \pm 0.6 \times 10^{11}$ [cm ³ ·mol ⁻¹ ·s ⁻¹]
$E_{P_{700}^+/P_{700}}^{0'}$		0.66 ± 0.14 [V vs Ag/AgCl]
$E_{F_B/F_B^-}^{0'}$		-0.27 ± 0.17 [V vs Ag/AgCl]

at the surface, and causes the current to decrease approximately as $t^{-1/2}$.³⁹ During each experiment, the electrode was irradiated from $t = 50$ –70 s. From these data, we observed that the direction and magnitude of the photocurrent to be dependent upon the overpotential, with anodic responses observed at $\eta \geq -0.022$ V and cathodic responses at $\eta \leq -0.042$ V.

Numerical Solution and Parameter Extraction Results. The system of ordinary and partial differential equations that comprised the model was solved using Matlab's numerical PDE solver "pdepe". The surface concentrations, that is, the concentrations at $x = 0$, obtained from the solutions to these equations were used to calculate a simulated current density by eq 17. Kinetic parameters were extracted from experimental data by using the Matlab function "fminsearch" to minimize the residual between the measured current density and the simulated current density at corresponding conditions by iteratively varying the unknown kinetic parameters in the model. Parameters were obtained from the experiments performed at each overpotential, and the mean and standard deviations of these parameters are presented in Table 1.

First, kinetic parameters that described the heterogeneous reaction of the electrochemical mediator (i.e., k_M^0 and α_M , the standard rate constant and the charge transfer coefficient of the electrochemical mediator, respectively) were obtained from experimental periods during which the electrode was not irradiated. These "dark" experimental conditions allowed for the kinetics that governed the mediator/electrode reactions to be decoupled from interactions between the photogenerated reaction centers of PSI. The standard rate constant for the $\text{Fe}(\text{CN})_6^{3-/4-}$ in the present system was determined to be $9.6 \pm 0.5 \times 10^{-4}$ cm·s⁻¹, which is lower than previously reported values of 3 – 31×10^{-3} cm·s⁻¹ for this parameter in similar electrochemical systems at unmodified gold electrodes,⁴⁰ which is likely due to charge-transfer resistances imparted to the electrode surface by the SAM and adsorbed protein film. The charge transfer coefficient of the electrochemical mediator exhibited some dependence on overpotential, and this behavior was represented in the model using a logistic function that was obtained empirically from the data (details are presented in Supporting Information).

Once the kinetic parameters that described the heterogeneous electron transfer reactions between the electrochemical mediator and the electrode were obtained, they were entered into the simulation to allow for the extraction of the parameters that governed the reactions involving the photogenerated reaction centers of PSI. These "light" parameters were similarly extracted from the photochronoamperometric data by fitting the experiments performed at each overpotential individually. Figure 4a,b shows representative experimental data plotted with the simulated current densities obtained using the empirical parameters extracted from the data. One limitation of the present model is that nonfaradaic currents associated with charging and reordering of the electronic double layer in response to changes in the local electronic environment at the electrode surface are not accounted for. These nonfaradaic phenomena likely account for disparities between experimental and simulated current densities observed immediately following the onset of irradiation, as shown in Figure 4a,b. Once parameters were individually obtained from the experiments performed at each overpotential investigated, their mean values (reported in Table 1) were put back into the simulation and used to generate a surface plot that displays the simulated current density over the entire range of overpotentials. This plot is presented in Figure 4c, and the experimental data, also plotted as a surface, are shown in Figure 4d.

With the exception of the formal potentials of the P_{700} and F_B reaction centers of PSI (denoted $E_{P_{700}^+/P_{700}}^{0'}$ and $E_{F_B/F_B^-}^{0'}$, respectively), the units of the extracted parameters prohibit their direct comparison to previously reported values in the literature as a result of the nature of the mechanistic model employed in this work. The aforementioned formal potentials were determined to be $+0.69 \pm 0.14$ and -0.28 ± 0.17 V versus Ag/AgCl for $E_{P_{700}^+/P_{700}}^{0'}$ and $E_{F_B/F_B^-}^{0'}$, respectively. These values are ~ 400 mV more positive than previous reports of these parameters, as determined by electron paramagnetic resonance⁴¹ (EPR) and optical redox titrations;⁴² however, previous electrochemical measurements of these parameters from PSI in lipid films on electrode surfaces⁴³ yielded values that were 200–300 mV more positive than those obtained by other techniques, and the positive shift was attributed to the changes in local electronic environment of the reaction centers imparted by the polarized electrode and electronic double layer at the electrode/electrolyte interface. As these nonfaradic electrochemical processes are neglected in the present model, they are likely responsible for the observation of the positive shift observed in the formal potentials of the reaction centers of PSI obtained by comparing this simulation to the experimental data set. Nevertheless, the energetic difference between the formal potentials of the reaction centers obtained in this work of ~ 1 V remains consistent with those obtained by other methods in different systems.

Current Contributions and PSI Orientation. Once the simulation parameters were obtained from the experimental data, the simulation was used to investigate the contribution of the various heterogeneous electrochemical reactions to the net current density of the system. The net current density as calculated by eq 17 can be decomposed into contributions by heterogeneous electron transfer between the electrode and the electrochemical mediators, P_{700} reaction centers, and F_B iron sulfur clusters. These various contributions were investigated by calculating the individual current densities resulting from a simulation performed at an overpotential of 0.088 V (individual empirical parameters obtained from the corresponding experiment conducted at $\eta = 0.088$ V were used for this investigation, rather than the

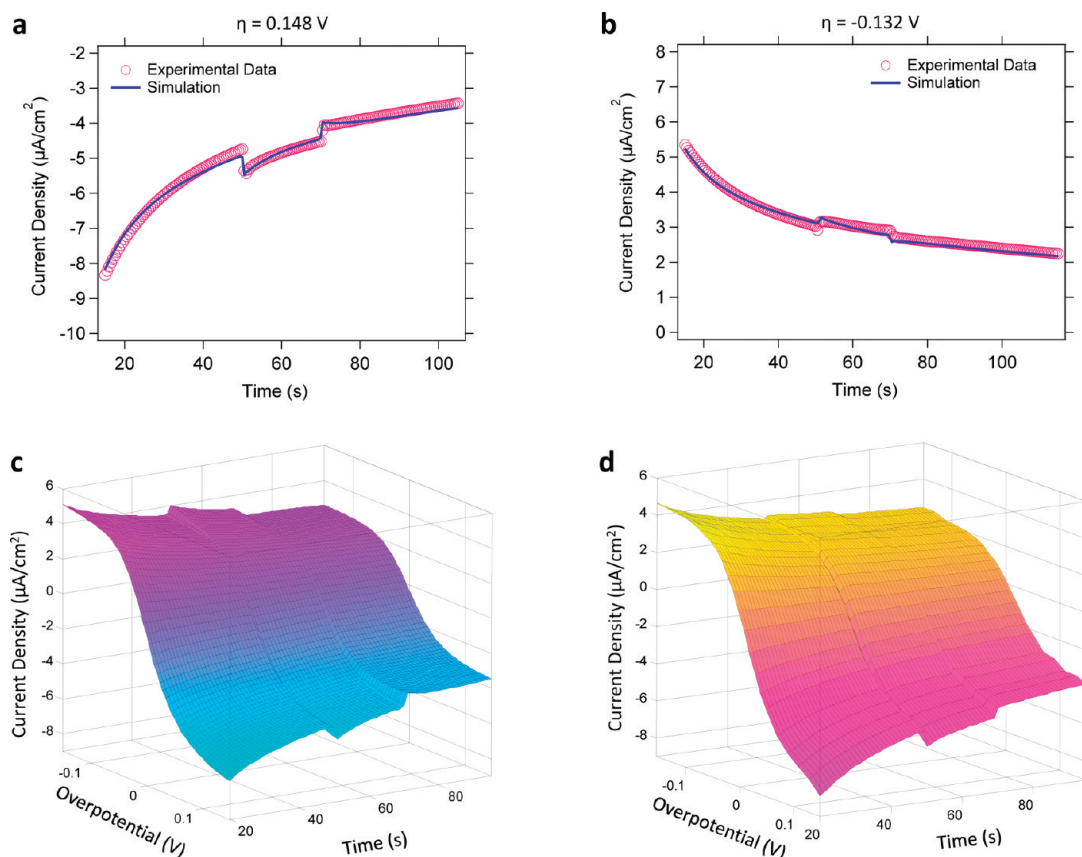


Figure 4. Simulated current densities produced using parameters extracted from corresponding photochronoamperometric experiments are shown in (a) and (b). Parameters were obtained from each chronoamperometric experiment individually, and their mean averages were input into the simulation and used to generate a surface plot that describes the current density continuously over the range of investigated potentials (c). The experimental data are shown as a surface plot for comparison in (d).

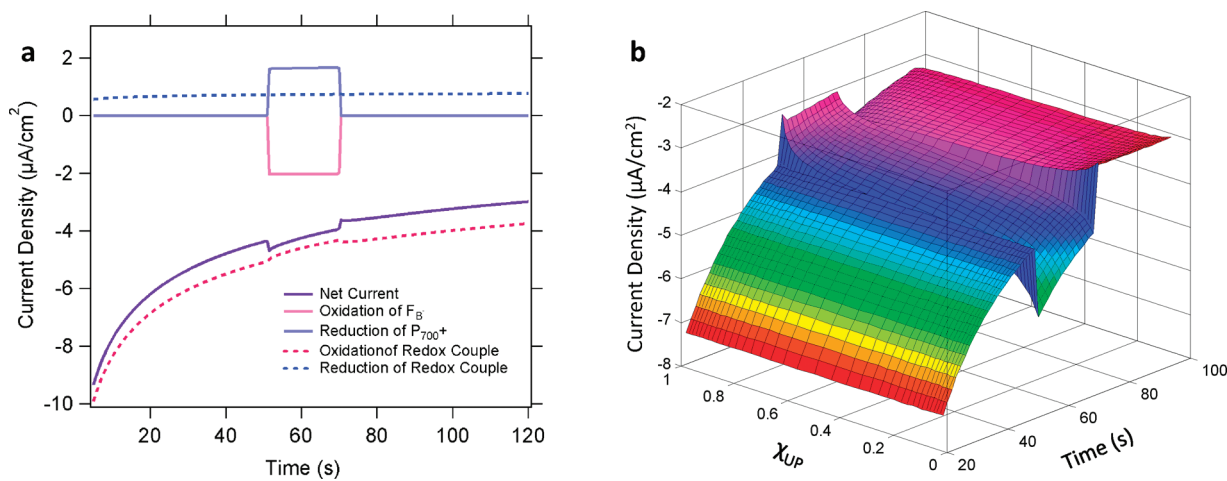


Figure 5. (a) At overpotentials where both anodic and cathodic current components contribute to the net current density, the simulation predicts that the majority of the photocurrent produced by the PSI monolayer cancels because of its opposite direction. The simulation shown in (a) was performed using an overpotential of 0.088 V . (b) The orientation factor of PSI was varied from $\chi_{up} = 0-1$, assuming that $\chi_{up} + \chi_{down} = 1$ in the chronoamperometric simulation at $\eta = 0.088 \text{ V}$. The model predicts that the net photocurrent density is dictated predominantly by kinetics at this overpotential for orientations between 20 and 80%; however, orienting $\geq 90\%$ of the PSI complexes in a single configuration will produce significant enhancements to photocurrent even at overpotentials where oxidation and reduction of the reaction centers of PSI are both favorable.

average parameters, to more accurately reflect the photocurrent contributions present in the corresponding experiment). These current density contributions are shown in Figure 5a. At this over-

potential, a net anodic current flows but still contains a cathodic contribution from reduction of the redox couple. Both experiment and simulation display a net anodic photocurrent production at this

overpotential; however, the simulation predicts large photocurrent contributions from the PSI film in both anodic and cathodic directions, with a slightly stronger response in the anodic direction that gives rise to the anodic net photocurrent. To provide further insight into these competing photocurrents, the effect of the orientation of the PSI complexes on the net photocurrent was investigated by varying the orientation fractions, χ_{up} and χ_{down} . The same simulation at an overpotential of 0.088 V was performed while varying χ_{up} , the fraction of PSI complexes oriented such that their P_{700} reaction centers were electronically accessible to the electrode, from 0–1, and the predicted current densities are presented in Figure 5b. These results show relatively small net photocurrents when only 20–80% of the PSI complexes are similarly oriented due to the competing directionalities of the photocurrents, while considerably larger photocurrents are predicted in both anodic and cathodic directions when 90% or more of the PSI complexes are similarly oriented. These results suggest that net photocurrent is dictated predominantly by electrochemical kinetics in the 20–80% orientation regime, but that similarly orienting $\geq 90\%$ of the PSI complexes will produce significant photocurrent enhancements even at photocurrents at which the heterogeneous reduction of P_{700}^+ and oxidation of F_B^- are both energetically feasible. This analysis predicts that achieving high degrees of orientation in PSI monolayer systems will produce orders of magnitude more photocurrent than a system in which PSI complexes are randomly oriented and suggests the demonstration of this large photocurrent enhancement as an evidential criterion for orientation strategies claimed to produce orientations of $\geq 90\%$.

CONCLUSIONS

In summary, we have developed a mechanistic, kinetic model for the photocurrent production by an electrode modified by a PSI monolayer in the presence of electrochemical mediators. Kinetic and electrochemical parameters were obtained by minimizing the residual between the current densities predicted by the model to photochronoamperometric experiments performed over a range of overpotentials. The empirically obtained parameters that described the behavior of the system in dark conditions predicted current densities that were in good agreement with the experimental data. Parameters describing the photoelectrochemical behavior of PSI were also obtained, and the average values of these parameters were used to yield a model that was continuous over the range overpotentials investigated. Discrepancies between simulation and experiment observed after the onset of irradiation likely arose from nonfaradaic currents associated with reordering of the electric double layer, which were not accounted for in the present model. The completed simulation was used to investigate contributions to the current density and predicted that the majority of the photocurrent produced by the PSI monolayer cancels unless $\sim 80\%$ or more of the protein complexes are oriented in a similar configuration with respect to the electrode surface. The mathematical framework developed in this work could be further generalized in future studies by considering the intermediate electron transfer steps within PSI, which would help to decouple the kinetics that govern electron transfer between the reaction centers of PSI and electrochemical mediators from the kinetics of the charge separation and intraprotein electron transfer. The accuracy of the extracted parameters may also be improved by employing more modern extraction and purification techniques to improve the integrity of the PSI complexes.

ASSOCIATED CONTENT

S Supporting Information. Additional optical characterizations of the electrochemical system, including absorbance spectra of the PSI suspension and electrochemical mediators, as well as the emission spectrum of the light source used to irradiate the system, are shown. Discussion of the quantification of the optical parameters in the model is included. Development of PDEs for the transport and heterogeneous reactions of electrochemical mediators is presented with a representative graphical solution. A discussion of the overpotential dependence of the transfer coefficient for the electrochemical mediator is included and the empirical, logistic fit used to model this behavior is presented. This material is available free of charge via the Internet at <http://pubs.acs.org>.

AUTHOR INFORMATION

Corresponding Author

*Tel.: 303-384-7615. Fax: 303-384-7752. E-mail: peter.ciesielski@nrel.gov

ACKNOWLEDGMENT

We gratefully acknowledge financial support from the National Science Foundation (DMR 0907619) and an IGERT fellowship (NSF 0333392) for P.N.C. We also acknowledge support for this project during the editing of this manuscript from a NSF RII grant (NSF EPSCoR EPS 1004083) for G.K.J. and D.E.C. and a Scialog award from the Research Corporation for Science Advancement for D.E.C.

REFERENCES

- (1) Govindjee. Milestones in Photosynthesis Research. In *Probing Photosynthesis Mechanisms, Regulation, and Adaptation*; Yunus, M., Pathre, U., Mohanty, P., Eds.; Taylor & Francis: London, 2000.
- (2) Nelson, N. *J. Nanosci. Nanotechnol.* **2009**, *9*, 1709.
- (3) Brettel, K.; Leibl, W. *Biochim. Biophys. Acta, Bioenerg.* **2001**, *1507*, 100.
- (4) Amunts, A.; Drory, O.; Nelson, N. *Nature* **2007**, *447*, 58.
- (5) Terasaki, N.; Yamamoto, N.; Tamada, K.; Hattori, M.; Hiraga, T.; Tohri, A.; Sato, I.; Iwai, M.; Iwai, M.; Taguchi, S.; Enami, I.; Inoue, Y.; Yoshinori, Y.; Yonezawa, T.; Mizuno, K.; Murata, M.; Hiroshi, N.; Yoneyama, S.; Minakata, M.; Ohmori, T.; Sakai, M.; Fujii, M. *Biochim. Biophys. Acta, Bioenerg.* **2007**, *1767*, 653.
- (6) Faulkner, C. J.; Lees, S.; Ciesielski, P. N.; Cliffel, D. E.; Jennings, G. K. *Langmuir* **2008**, *24*, 8409.
- (7) Ciesielski, P. N.; Scott, A. M.; Faulkner, C. J.; Berron, B. J.; Cliffel, D. E.; Jennings, G. K. *ACS Nano* **2008**, *2*, 2465.
- (8) Terasaki, N.; Yamamoto, N.; Hiraga, T.; Sato, I.; Inoue, Y.; Yamada, S. *Thin Solid Films* **2006**, *499*, 153.
- (9) Terasaki, N.; Yamamoto, N.; Hiraga, T.; Yamanoi, Y.; Yonezawa, T.; Nishihara, H.; Ohmori, T.; Sakai, M.; Fujii, M.; Tohri, A.; Iwai, M.; Inoue, Y.; Yoneyama, S.; Minakata, M.; Enami, I. *Angew. Chem. Int. Ed.* **2009**, *48*, 1585.
- (10) Lee, J. W.; Greenbaum, E. *Appl. Biochem. Biotechnol.* **1995**, *51*–2, 295.
- (11) Carmeli, I.; Frolov, L.; Carmeli, C.; Richter, S. *J. Am. Chem. Soc.* **2007**, *129*, 12352.
- (12) Carmeli, I.; Mangold, M.; Frolov, L.; Zebli, B.; Carmeli, C.; Richter, S.; Holleitner, A. W. *Adv. Mater.* **2007**, *19*, 3901.
- (13) Das, R.; Kiley, P. J.; Segal, M.; Norville, J.; Yu, A. A.; Wang, L. Y.; Trammell, S. A.; Reddick, L. E.; Kumar, R.; Stellacci, F.; Lebedev, N.; Schnur, J.; Bruce, B. D.; Zhang, S. G.; Baldo, M. *Nano Lett.* **2004**, *4*, 1079.
- (14) Frolov, L.; Rosenwaks, Y.; Carmeli, C.; Carmeli, I. *Adv. Mater.* **2005**, *17*, 2434.

- (15) Frolov, L.; Rosenwaks, Y.; Richter, S.; Carmeli, C.; Carmeli, I. *J. Phys. Chem. C* **2008**, *112*, 13426.
- (16) Frolov, L.; Wilner, O.; Carmeli, C.; Carmeli, I. *Adv. Mater.* **2008**, *20*, 263.
- (17) Ciobanu, M.; Kincaid, H. A.; Lo, V.; Dukes, A. D.; Jennings, G. K.; Cliffel, D. E. *J. Electroanal. Chem.* **2007**, *599*, 72.
- (18) Proux-Delrouyre, V.; Demaille, C.; Leibl, W.; Setif, P.; Bottin, H.; Bourdillon, C. *J. Am. Chem. Soc.* **2003**, *125*, 13686.
- (19) Ke, B. *Plant Physiol.* **1967**, *42*, 1310.
- (20) Lee, J. W.; Collins, R. T.; Greenbaum, E. *J. Phys. Chem. B* **1998**, *102*, 2095.
- (21) Kolthoff, I. M.; Tomsicek, W. J. *J. Phys. Chem.* **1935**, *39*, 945.
- (22) Amunts, A.; Drory, O.; Nelson, N. *Nature* **2007**, *447*, 58.
- (23) Deen, W. M. *Analysis of Transport Phenomena*; Oxford University Press: Oxford, NY, 1998.
- (24) Boekema, E. J.; Wynn, R. M.; Malkin, R. *Biochim. Biophys. Acta* **1990**, *1017*, 49.
- (25) Fotiadis, D.; Muller, D. J.; Tsiotis, G.; Hasler, L.; Tittmann, P.; Mini, T.; Jeno, P.; Gross, H.; Engel, A. *J. Mol. Biol.* **1998**, *283*, 83.
- (26) Lee, J. W.; Lee, I.; Laible, P. D.; Owens, T. G.; Greenbaum, E. *Biophys. J.* **1995**, *69*, 652.
- (27) Díaz-Quintana, A.; Leibl, W.; Bottin, H.; Sétif, P. *Biochemistry* **1998**, *37*, 3429.
- (28) Vassiliev, I. R.; Jung, Y.-S.; Yang, F.; Golbeck, J. H. *Biophys. J.* **1998**, *74*, 2029.
- (29) Trissl, H. W.; Wilhelm, C. *Trends Biochem. Sci.* **1993**, *18*, 415.
- (30) Lee, J. W. Excitation transfer dynamics and P700 photooxidation kinetics in isolated photosystem I. *Ph.D. Dissertation*, Cornell University, NY, 1993.
- (31) Vassiliev, I. R.; Jung, Y.; Mamedov, M. D.; Semenov, A. Y.; Golbeck, J. H. *Biophys. J.* **1997**, *72*, 301.
- (32) Bard, A. J.; Faulkner, L. R. *Electrochemical Methods: Fundamentals and Applications*, 2nd ed.; Wiley: New York, 2001.
- (33) Kincaid, H. A.; Niedringhaus, T.; Ciobanu, M.; Cliffel, D. E.; Jennings, G. K. *Langmuir* **2006**, *22*, 8114.
- (34) Reeves, S. G.; Hall, D. O. *Methods Enzymol.* **1980**, *69*, 85.
- (35) Ciobanu, M.; Kincaid, H. A.; Jennings, G. K.; Cliffel, D. E. *Langmuir* **2005**, *21*, 692.
- (36) Baba, K.; Itoh, S.; Hastings, G.; Hoshina, S. *Photosynth. Res.* **1996**, *47*, 121.
- (37) Shiozawa, J. A.; Alberte, R. S.; Thornber, J. P. *Arch. Biochem. Biophys.* **1974**, *165*, 388.
- (38) Porra, R. J. *Photosynth. Res.* **2002**, *73*, 149.
- (39) Cottrell, F. G. Z. *Phys. Chem.* **1902**, *42*.
- (40) Marecek, V.; Samec, Z.; Weber, J. *J. J. Electroanal. Chem.* **1978**, *94*, 169.
- (41) Brettel, K. *Biochim. Biophys. Acta, Bioenerg.* **1997**, *1318*, 322.
- (42) Jordan, R.; Nessau, U.; Schlodder, E. *Photosynthesis: Mechanism and Effects*; Kluwer Academic Publishers: Dordrecht, 1998; Vol. 1.
- (43) Munge, B.; Das, S. K.; Ilagan, R.; Pendon, Z.; Yang, J.; Frank, H. A.; Rusling, J. F. *J. Am. Chem. Soc.* **2003**, *125*, 12457.